Binarizing Weights Wisely for Edge Intelligence: Guide for Partial Binarization of Deconvolution-Based Generators

Jinglan Liu, Jiaxin Zhang, Yukun Ding, Xiaowei Xu, *Member, IEEE*, Meng Jiang, and Yiyu Shi, *Senior Member, IEEE*

***Abstract*—This article explores the weight binarization of the deconvolution-based generator in a generative adversarial network (GAN) for memory saving and speedup of image construction on the edge. This article suggests that different from convolutional neural networks (including the discriminator) where all layers can be binarized, only some of the layers in the generator can be binarized without significant performance loss. Supported by theoretical analysis and verified by experiments, a direct metric based on the dimension of deconvolution operations is established, which can be used to quickly decide which layers in a generator can be binarized. Our results also indicate that both the generator and the discriminator should be binarized simultaneously for balanced competition and better performance during training. The experimental results on CelebA dataset with DCGAN and original loss functions suggest that directly applying state-of-the-art binarization techniques to all the layers of the generator will lead to 2.83× performance loss measured by sliced Wasserstein distance compared with the original generator, while applying them to selected layers only can yield up to 25.81× saving in memory consumption, and 1.96× and 1.32× speedup in inference and training, respectively, with little performance loss. Similar conclusions can also be drawn on other loss functions for different GANs.**

***Index Terms*—Binarization, compact model, compression, deconvolution, generative adversarial network (GAN).**

I. Introduction

GENERATIVE adversarial networks (GANs), which are spin-offs from conventional convolutional neural networks (CNNs), have attracted much attention in the fields of reinforcement learning, unsupervised learning and also semi-supervised learning [1]–[3]. A GAN is composed of two parts: 1) a discriminator and 2) a generator. Usually, discriminators are implemented by CNNs, while generators are implemented by deconvolutional neural networks. More details about GANs will be presented in Section II-B.

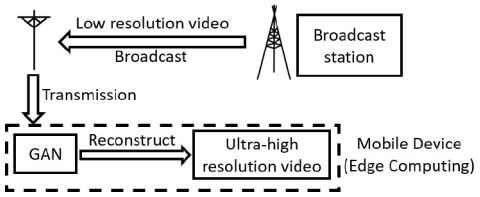

Fig. 1. Low resolution broadcast based on GAN.

Some promising applications based on GANs include images reconstruction with super-resolution, art creation, and image-to-image translation [4], many of which can run on mobile devices (edge computing). For example, one potential application of GANs allow videos to be broadcast in low resolution and then reconstructed to ultrahigh resolution by end users [5] as shown in Fig. 1.

However, the resources required by GANs to perform computations in real-time may not be easily accommodated by mobile devices. For example, constructing an image of 64×64 resolution with deep convolutional generative adversarial network (DCGAN) [6] requires 86.6 MB of memory, most of which is used for the generator. The memory goes up to 620.8 MB for 1024×1024 resolution [7], and up to about 800 MB for the popular 4K video with resolution of 3840×2160. On the other hand, one of the state-of-the-art mobile processors, A12 Bionic in the newest iPhone XS Max [8], provides only 4 GB RAM, most of which must be occupied by the operating system and its peripheries. As a result, developers must restrict neural network models to just a few megabytes to avoid crash [9]. The memory budget gets even tighter when it comes to mobile devices of smaller form factor such as Apple Watch series 3, which only has 768 MB RAM.

The same problem has been well known for conventional CNNs, and various solutions have been proposed via redesigning the algorithms and/or computation structures [10]–[13]. Among them, quantization until the binary is one of the most popular techniques as it fits the hardware implementation well with high efficiency [9], [14], [15]. However, quantization can

Manuscript received September 22, 2019; revised January 19, 2020; accepted March 4, 2020. Date of publication March 26, 2020; date of current version November 20, 2020. This work was supported in part by the National Science Foundation under Grant CCF-1919167 and Grant CNS-1822099. This article was recommended by Associate Editor H. Li. *(Corresponding author: Yiyu Shi.)*

Jinglan Liu, Yukun Ding, Meng Jiang, and Yiyu Shi are with the Department of Computer Science and Engineering, University of Notre Dame, Notre Dame, IN 46556 USA (e-mail: jliu16@nd.edu; yding5@nd.edu; mjiang2@nd.edu; yshi4@nd.edu).

Jiaxin Zhang was with the University of Science and Technology of China, Hefei 230026, China. He is now with Horizon Robotics, Beijing 100190, China.

Xiaowei Xu is with the Guangdong Cardiovascular Institute, Guangdong Provincial Key Laboratory of South China Structural Heart Disease, Guangdong Provincial People's Hospital, Guangdong Academy of Medical Sciences, Guangzhou 510080, China.

Digital Object Identifier 10.1109/TCAD.2020.2983370

reduce the expressive power of the neural networks significantly and the discrete parameters make the optimization much more difficult. Naive quantization usually leads to total failure, especially, for binarization. Significant effort has been devoted to develop better quantization and binarization methods, as well as the hardware accelerator [14], [16]–[19]. Its success on CNNs has been demonstrated by multiple works, where memory consumption is deeply compressed although sometimes the performance cannot be preserved [20]–[23].

Compression techniques can be readily applied to discriminator networks in GANs, which are nothing different from conventional CNNs. It may be alluring to also apply the quantization techniques to binarize generators, especially, the deconvolution-based [24] ones as the computation the process looks similar. However, instead of distilling local information from a global map as in convolution operations, deconvolution attempts to construct the global map by local information. This difference can lead to significantly different binarization results, as will be discussed in Section III. Accordingly, a scheme tailored to deconvolution-based generators is warranted.

In this article, we show through theoretical analysis that under certain conditions, binarizing a deconvolution layer may cause significant performance loss, which also happens in compression of CNNs per empirical findings so far. Since there is no explanation for this phenomenon to the best of the authors' knowledge, an intuitive guess is that not all layers can be binarized together while preserving performance. Thus, some layers need to stay in the format of floating point for performance, while others can be binarized without affecting performance. To quickly decide whether a layer can be binarized, supported by theoretical analysis and verified by experiments, a simple yet effective metric based on the dimension of deconvolution operations is established. Based on this metric, we can make use of existing compression techniques to binarize the generator of GANs with little performance loss. We then propose the scheme of partial binarization of deconvolution-based generators (PBGen) under the guide of the metric.

Furthermore, we find that only binarizing the generator and leaving discriminator network unchanged will introduce unbalanced competition and performance degradation. Thus, both networks should be binarized at the same time. The experimental results based on CelebA suggest that directly applying state-of-the-art binarization techniques to all the layers of the generator will lead to $2.83\times$ performance loss measured by sliced Wasserstein distance (SWD) compared with the original generator, while applying them to selected layers only can yield up to $25.81\times$ saving in memory consumption, and $1.96\times$ and $1.32\times$ speedup in inference and training, respectively, with little performance loss. The conclusions will stay the same even though different loss functions are utilized.

The remainder of this article is organized as follows. Section II discusses related work and background for compression techniques for CNN, as well as GANs. Section III exhibits the theoretical analysis on the power of representation in deconvolution/convolution layers and the algorithm for model binarization based on it. Experiments for verification and performance are displayed in Section IV. This article is concluded in Section V.

II. Related Work and Background

A. CNN Compression

Compression techniques for CNNs mainly consist of pruning, quantization, restructure, and other approximations based on mathematical matrix manipulations [10], [25], [26]. The main idea of the pruning method in [21] is to "prune" connections with smaller weights out so that both synapses and neurons are possible to be removed from the original structure. This can work well with traditional CNNs and reduce the number of parameters of AlexNet by a factor of nine [21]. Restructure methods modify network structures for compression, such as changing functions or block order in layers [20], [26].

In this article, we focus on the quantization technique. Quantization aims to use fewer bits to present values of weights or even inputs. It has been used to accelerate CNNs in various works at different levels [27]–[29], including ternary quantization [16], [30] and iterative quantization [31], with small loss. Han *et al.* [10] proposed to determine weight sharing after a network is fully trained, so that the shared weights approximate the original network. From a fully trained model, weights are clustered and replaced by the centroids of clusters. During retraining, the summation of the gradients in the same groups are used for the fine-tuning of the centroids. Through such quantization, it is reported to be able to compress AlexNet up by around 8% before significant accuracy loss occurs. If the compression rate goes beyond that, the accuracy will deteriorate rapidly.

Numerous recent work [14], [20], [23], [32]–[35] pushed it further by using binarization to compress CNNs, where only a single bit is used to represent values. Training networks with weights and activations constrained to ± 1 was first proposed in [33]. Through transforming 32-bit floating point weight values to binary representation, CNNs with binary weights and activations are about $32\times$ smaller. In addition, when weight values are binary, convolutions can be estimated by only addition and subtraction without multiplication, which can achieve around $2.0\times$ speedup. However, the method introduces significant performance loss. To alleviate the problem, [20] proposed binary-weight-network (BWN), where all weight values are binarized with an additional continuous scaling factor for each output channel. We will base our discussion on this weight binarization afterward, which is one of the state-of-the-art binarization methods.

Most recently, hybrid quantization has attracted more and more attention, because it enables better tradeoff between compression and performance [36]–[38]. As for partial binarization, a subarea of hybrid quantization, on which we are focused, both training methods [39] and the corresponding hardware accelerators [19], [40] are also investigated extensively. The actual performance after compression heavily depends on the configuration of the partial binarization, i.e., which layers are binarized while others are not. Given the fact that the search space is too large to do exhaustive search, finding the optimal or near-optimal configuration becomes a foremost challenge. Chakraborty *et al.* [41] showed that adding full precision residual connections helps to reduce the loss of classification accuracy while getting

excellent memory compression. One potential drawback of this method is that it introduces additional memory overhead. Zhuang *et al.* [39] presented flexible network binarization with layer-wise priority, which is defined by the inverse of layer depth empirically. Prabhu *et al.* [42] proposed to use the binarization error of each layer as the indication of its importance to the final performance. They empirically show that partial binarization leads to significant improvement over fully binarized models. Very recently, Chakraborty *et al.* [43] also utilized principal component analysis (PCA) to identify significant layers in CNNs and uses higher precision on important layers. However, this method depends on pretrained models, and PCA contains a large amount of computation naturally.

All things considered, none of the existing work explored the compression of generators in GANs, where deconvolution replaces convolution as the major operation. Note that while there is a recent work that uses the term of "binary generative adversarial networks" [44], it is not about the binarization of GANs. In that work, only the inputs of the generator are restricted to binary code to meet the specific application requirement. All parameters inside the networks and the training images are not quantized.

B. GAN

GAN was developed by [45] as a framework to train a generative model by an adversarial process. In a GAN, a discriminative network (discriminator) learns to distinguish whether a given instance is real or fake, and a generative network (generator) learns to generate realistic instances to confuse the discriminator.

Originally, the discriminator and the generator of a GAN are both multilayer perceptrons. Researchers have since proposed many variants of it. For example, DCGAN transformed multilayer perceptrons to deep convolutional networks for better performance. Specifically, the generator is composed by four deconvolutional layers. GANs with such a convolutional/deconvolutional the structure have also been successfully used to synthesize plausible visual interpretations of given text [46] and to learn interpretable and disentangled representation from images in an unsupervised way [47]. Wasserstein generative adversarial networks (WGANs) [48] and least-squares generative adversarial networks (LSGANs) [49] have been proposed with different loss functions to achieve more stable performance, yet they both employed the deconvolution operations too. To verify the robustness of our analysis, both DCGAN and LSGAN are tested in our experiments.

III. Analysis on Power of Representation

In this section, to decide whether a layer can be binarized, we analyze the power of a deconvolution layer to represent any given the mapping between the input and the output, and how such power will affect the performance after binarization. We will show that the performance loss of a layer is related to the dimension of the deconvolution, and develop a metric called the degree of redundancy to indicate the loss. Finally, based on the analysis, several inferences are deduced at the end of this section, which should lead to effective and efficient binarization.

In the discussion below, we ignore batch normalization as well as activation operations and focus on the deconvolution operation in a layer, as only the weights in that operation are binarized. The deconvolution process can be transformed to equivalent matrix multiplication. Let $\mathbf{D}^I$ ($\in \mathcal{R}^{c_i \times h_i \times w_i}$, where c_i, h_i, and w_i are number of channels, height, and width of the input, respectively) be the input matrix, and $\mathbf{D}^O$ ($\in \mathcal{R}^{c_o \times h_o \times w_o}$, where c_o, h_o, and w_o are the number of channels, height and width of the output, respectively) be the output matrix. Denote $\mathbf{K}$ ($\in \mathcal{R}^{c_i \times c_o \times h_k \times w_k}$, where h_k and w_k are the height and width of a kernel in the weight matrix) as the weight matrix to be deconvoluted with $\mathbf{D}^I$. Padding is ignored in the discussion, since it will not effect the results.

For the deconvolution operation, the local regions in the output can be stretched out into columns, by which we can cast $\mathbf{D}^O$ to $\mathbf{D}^{Od} \in \mathcal{R}^{s_i \times r_o}$, where $s_i = h_i w_i$, $r_o = c_o h_k w_k$. Similarly, $\mathbf{D}^{Id} \in \mathcal{R}^{s_i \times c_i}$ can be restructured from $\mathbf{D}^I$, and $\mathbf{K}^d \in \mathcal{R}^{c_i \times r_o}$ can be restructured from $\mathbf{K}$, where $s_i = h_i w_i$, $r_o = c_o h_k w_k$. Please refer to [50] for details about the transform. Then, the deconvolution operation can be compactly written as

$$\mathbf{D}^{Od} = \mathbf{D}^{Id} * \mathbf{K}^d \tag{1}$$

where $*$ denotes matrix multiplication. $\mathbf{D}^{Id}$ and $\mathbf{D}^{Od}$ are the matrices containing pixels for an image or an intermediate feature map. During the training process, we adjust the values of $\mathbf{K}^d$ to construct a desired the mapping between $\mathbf{D}^{Id}$ and $\mathbf{D}^{Od}$.

We use $(\cdot)_j$ to denote the jth column of a matrix. Then (1) can be decomposed column-wise as

$$\mathbf{D}^{Od}_j = \mathbf{D}^{Id} * \mathbf{K}^d_j, \quad 1 \le j \le r_o \tag{2}$$

where $\mathbf{K}^d_j \in \mathcal{R}^{c_i}$ and $\mathbf{D}^{Od}_j \in \mathcal{R}^{s_i}$.

Now, we analyze a mapping between an arbitrary input $\mathbf{D}^{Id}$ and an arbitrary output $\mathbf{D}^{Od}_j$. From (2), when the weights are continuously selected, all vectors that can be expressed by the right-hand expression is a subspace Ω spanned by the columns of $\mathbf{D}^{Id}$, the dimension of which is c_i. Here, we have assumed without loss of generality that $\mathbf{D}^{Id}$ has full column rank. When $c_i < s_i$, which is the dimension of the output space Φ where $\mathbf{D}^{Od}_j$ lies, Ω is of lower dimension than Φ, and accordingly, $\mathbf{D}^{Od}_j$ can either be uniquely expressed as a linear combination of the columns in $\mathbf{D}^{Id}$ if it lies in Ω (i.e., a unique $\mathbf{K}^d_j$ exists), or cannot be expressed if it is not (i.e., no such $\mathbf{K}^d_j$ exists). When $c_i = s_i$, Ω and Φ are equivalent, and any $\mathbf{D}^{Od}$ can be uniquely expressed as a linear combination of the columns in $\mathbf{D}^{Id}$. When $c_i > s_i$, Ω and Φ are still equivalent, but any $\mathbf{D}^{Od}$ can be expressed as an infinite number of different linear combinations of the columns in $\mathbf{D}^{Id}$. In fact, the coefficients $\mathbf{K}^d_j$ of these combinations lie in a $(c_i - s_i)$-dimensional subspace Ψ.

The binarization imposes a constraint on the possible values of the elements in $\mathbf{K}^d_j$. Only finite number of combinations are possible. If $c_i \le s_i$, then at least one of these combinations has to be proportional to the unique $\mathbf{K}^d_j$ that yields the desired $\mathbf{D}^{Od}_j$ to preserve performance. If $c_i > s_i$, then one of

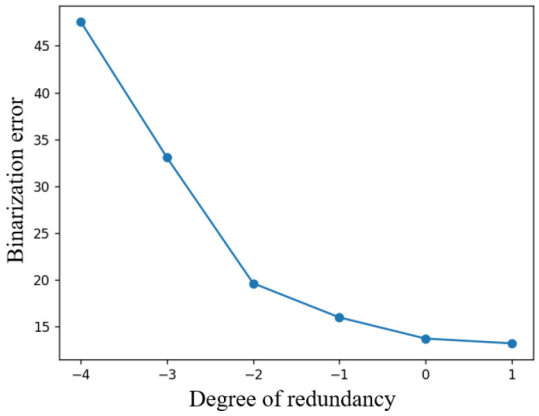

Fig. 2. Binarization error versus degree of redundancy for a deconvolution layer.

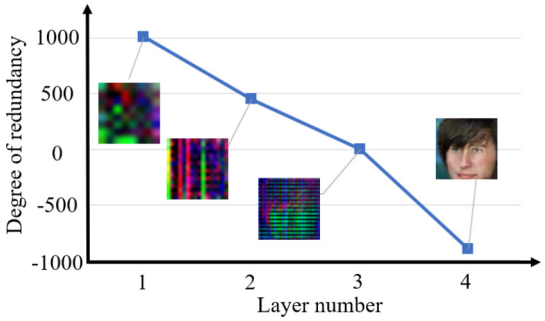

Fig. 3. Degree of redundancy versus layer number for DCGAN. The intermediate feature maps at the output of each layer as well as the final output are also presented.

these combinations needs to lie in the subspace Ψ to preserve performance. Apparently, the larger the dimension of Ψ is, the more likely this will happen, and the less the performance loss is. A detailed math analysis is straightforward to illustrate this, and is omitted here in the interest of space. Accordingly, we define the dimension of Ψ, $c_i - s_i$, as the degree of redundancy in the rest of this article. Note that when this metric is negative, it reflects that Ω is of lower dimension than Φ and thus this deconvolution the layer is more vulnerable to binarization errors. In general, a higher degree of redundancy should give lower binarization error.

We will use a small numerical example to partially validate the above discussion. We construct a deconvolution layer and vary its degree of redundancy by adjusting the c_i in it, where $s_i = 20$. For each degree of redundancy we calculate the minimum average Euclidean distance between the original output and the output produced by binarized weights, which reflects the error introduced through the binarization process, referred to as binarization error throughout this article. The binarization error is obtained by enumerating all the possible combinations of those binary weights. The results are depicted in Fig. 2. From the figure we can see that the error decreases with the increase of the degree of redundancy, which matches our conjecture.

For generators in most state-of-the-art GAN models [6], [49], we find that the degree of redundancy reduces with the increase in depth, eventually dropping below zero. Such a decrease reflects the fact that more details are generated at the output of a layer as its depth grows, as can also be seen in Fig. 3. These details are highly correlated, and reduce the subspace needed to cover then.

Based on our analysis, several inferences can be deduced to guide the binarization.

1) With the degree of redundancy, taking advantage of existing binarization methods becomes reasonable and feasible. Binarizing layers with higher degree of redundancy will lead to lower performance loss after binarization, while layers with negative degree of redundancy should be kept un-binarized to avoid excessive performance loss.
2) According to the chain rule of probability in directed graphs, the output of every layer is only dependent on its direct input. Therefore, the binarizability of each layer can be superposed. If a layer can be binarized alone, it can be binarized with other such layers.
3) When binarizing several deconvolution layers together, the layer with the least degree of redundancy may be the bottleneck of the generator's performance.

As a result, only shallower layer(s) of a generator can be binarized together to preserve its performance, because of the degree of redundancy trend in it. This leads to PBGen. Besides, such analysis may also explain why binarization can be applied in almost all convolution layers: distilling local information from a global map leads to positive degree of redundancy.

Under the guide of such inferences, the algorithm for wise binarization on Deconv/Conv networks can be implemented by calculating the degree of redundancy for every Deconv/Conv layer at first; then all these layers can be sorted by their degree of redundancy from high to low; in this order, every layer will be binarized singly to observe the difference in performance from the original full-precision version and whether to continue or not will be decided by the tradeoff between performance and efficiency; finally, selected layers will be binarized together to serve as the ultimate strategy for network binarization. This algorithm can be described as Algorithm 1. We attempt to preserve the original full-precision performance in our experiments.

In addition, following the same derivation process for deconvolution in this article, the degree of redundancy of a convolution layer can be defined as $w_k \times h_k \times c_i - c_o$, instead of $c_i - s_i$ for deconvolution. Usually in a convolution layer, $c_o = 2 \times c_i$, $w_k = h_k$, and $w_k = 3$ or 5. As a result, the degree of redundancy is usually positive, and convolution is more readily binarizable compared to deconvolution as well. This also explains why using 1×1 kernels will help compress networks while not hurting the networks' performance [51].

IV. Experiments

A. DCGAN and Different Settings

DCGAN will serve as a vehicle to verify the inferences deducted from the theoretical analysis in Section III. Except

Algorithm 1 Wise Binarization on Deconv/Conv Networks

$L \leftarrow$ number of Deconv/Conv layers
$T \leftarrow$ performance degradation threshold
for $l = 1 : L$ **do**
  Compute the degree of redundancy of each layer R_l
end for
$\mathbf{R} \leftarrow$ sorted $R_1 \cdots, R_L$ from high to low
$i \leftarrow 1$
while $i \leq L$ **do**
  Binarize the i-th layer
  if performance degradation exceeds T **then**
    break
  end if
  $i \leftarrow i + 1$
end while
return i
The network binarization strategy is to binarize the first $i-1$ layers according to $\mathbf{R}$ together

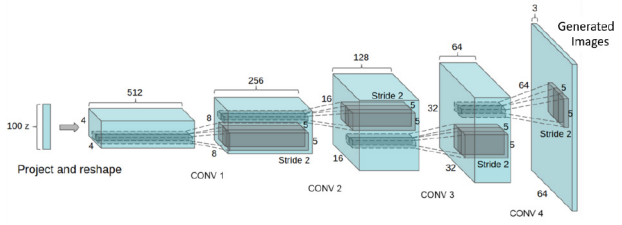

Fig. 4. Structure of the generators in DCGAN with dimension of each layer labeled. Deconvolutional layers are denoted as "CONV" (figure credit: [6]).

TABLE I
DEGREE OF REDUNDANCY IN EACH DECONVOLUTION LAYER OF THE GENERATOR IN DCGAN

Layer number	Label in Fig. 4	Degree of redundancy
1	CONV 1	496
2	CONV 2	192
3	CONV 3	-128
4	CONV 4	-960

for the original adversarial loss function for DCGAN, least-square loss function proposed in LSGAN is also tested in our experiments. The least-square loss is one of the most popular loss functions for GANs, because it has been proved to be efficient for different GANs training.

We will explore how to best binarize it with preserved performance. Specifically, we use the TensorFlow [52] implementation of DCGAN on GitHub [53]. The structure of its generator is illustrated in Fig. 4. The computed degree of redundancy in each layer in the generator is shown in Fig. 3 and qualitatively summarized in Table I. The degree of redundancy in the last layer drops to -960. According to the inferences before, we can expect that since the degree of redundancy decreases as the depth increases, binarizing shallower layers and keeping the deeper layers in the format of floating point will help preserve the performance. For the readers' information, the degrees of redundancy of the four convolution layers in the discriminator are 11, 1472, 2944, and 5888, respectively.

TABLE II
SETTINGS OF DIFFERENT PARTIAL BINARIZATION OF GENERATOR IN DCGAN

Setting	Layer(s) binarized	Discriminator binarized
A	None	N
B	1	N
C	2	N
D	3	N
E	4	N
F	1,2,3	N
G	1,2,3,4	N
H	1,2,3	Y

The binarization method used in BWNs proposed in [20] is adopted to binarize layers no matter in a generator network or in a discriminator network. In BWN, all the weight values are approximated with binary values. Through keeping floating-point gradients while training, BWN is able to trained from scratch without pretrain.

There are four deconvolution layers in total in the generator, and each layer can be either binarized or not. For verification, we have conducted experiments on all $2^4 = 16$ different settings, but only the eight representative ones are discussed for clarity and space, and others will lead us to the same conclusion. Those eight different representative settings are summarized in Table II for clearness. In this table, the "setting" column labels each setting. "layer(s) binarized" indicates which layer(s) are binarized in the generator. The "discriminator binarized" column tells whether the discriminator is binarized or not. "Y" means yes, while "N" means no. This column is introduced to verify an observation in our experiments to be discussed later. Although settings in experiments include unbinarized discriminator and binarized discriminator, whether the discriminator is binarized or not will not affect the generated images significantly. That is, if the generator cannot generate recognizable faces with the unbinarized discriminator, it still cannot generate any recognizable faces with a binarized discriminator; and *vice versa*.

Setting *G* will serve as the baseline model for performance after binarization, because it adopts the compression techniques based on CNNs directly without considering the degree of redundancy. On the other hand, Setting A serves as the baseline model when considering the memory saving, speedup, as well as performance difference before and after binarization, because it represents the original DCGAN in floating point representation. It is considered as one common GAN structure providing good performance.

B. Dataset and Metrics

CelebA [54] is used as the dataset for our experiments, because it is a popular and verified dataset for different GAN structures. DCGAN, WGAN, LSGAN, and many other GAN structures are tested on it [55]. As every image in CelebA contains only one face, it is much easier to tell the quality of the generated images.

Traditionally the quality of the generated images is identified by observation. However, qualitatively evaluation is always a hard problem. According to the in-depth analysis

Fig. 5. Images generated under different settings. (a) Setting A. (b) Setting B. (c) Setting C. (d) Setting D. (e) Setting E. (f) Setting F. (g) Setting G. (h) Setting H.

of commonly used criteria in [56], good performance in a single or extrapolated metric from average log-likelihood, Parzen window estimates, and visual fidelity of samples does not directly translate to good performance of a GAN. On the other hand, the log-likelihood score proposed in [57] only estimates a lower bound instead of the actual performance.

Very recently, Karras *et al.* [7] proposed an efficient metric, which we will use in our experiments, and showed that it is superior to MS-SSIM [58], which is a commonly used metric. It calculates the SWD between the training samples and the generated images under different resolutions. In particular, the SWD from the lower resolution patches indicates similarity in holistic image structures, while the finer-level patches encode information about pixel-level attributes. In this article, the max resolution is 64×64. Thus, according to [7], we will use three different resolutions to evaluate the performance: 16×16, 32×32, and 64×64. For all different resolutions, small SWD indicates that the distributions of the patches are similar, which means that a generator with smaller SWD is expected to produce images more similar to the images from the training samples in both appearance and variation.

C. Experimental Results

In this section, we will present experimental results that verify our inferences in Section III, along with some additional observations about the competition between the generator and the discriminator. The images generated by the original GAN (Setting A), in which all weights of each deconvolution layer are in the form of floating point, are displayed in Fig. 5(a). The images generated by the binarized DCGAN without considering the degree of redundancy are displayed in Fig. 5(g). These are our two baseline models.

1) Qualitative Comparison of Single-Layer Binarization: We start our experiments by comparing the images generated by binarizing a single layer in the generator of DCGAN. The results are shown in Fig. 5(b)–(e), which are generated by PBGen's under Setting B–Setting E, respectively. In other words, those PBGen's utilize binary weights to the first, the second, the third, and the last deconvolution layer, respectively. The degree of redundancy of each layer is shown in Fig. 3. From the generated figures we can then see that Fig. 5(b) generates the highest quality of images, similar to the original ones in Fig. 5(a). Images in Fig. 5(c) are slightly inferior to those in Fig. 5(b), but better than those in Fig. 5(d). Fig. 5(e) has no meaningful images at all. These observations are in accordance with our inferences in Section III: the performance loss when binarizing a layer is decided by its degree of redundancy, and a layer with negative degree of redundancy should not be binarized.

To address the concern that low performance of Setting E is caused by the low degree of redundancy instead of the position of the layer (the last layer), more experiments are conducted under Setting E. As analysed in Section III, degree of redundancy is defined by $c_i - s_i$, thus changing c_i of one layer will only change the degree of redundancy of that layer, and will not have an effect on other layers' degree of redundancy. Thus, experiments with different number of input channels for the CONV4 layer, c_4, under Setting E. The generated images of faces in these experiments are shown in Fig. 6. The original c_4 is 64, and experiments are also conducted with 128, 256, 512, and 1024, respectively. According to Table I, the degree of redundancy of CONV4 is zero when $c_4 = 1024$. As shown in Fig. 6, the generated images get clearer with more details along with the increased number of input channels and higher degree of redundancy.

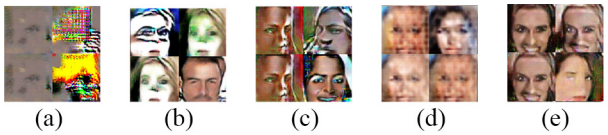

Fig. 6. Generated images of faces under Setting E with different number of input channels for the CONV4 layer. The number of the CONV4 layer for each experiments is (a) 64, (b) 128, (c) 256, (d) 512, and (e) 1024, respectively. With the increased number of input channels in the CONV4 layer, the degree of redundancy of this layer increases while other layers' degree of redundancy stays the same. This validates the degree of redundancy as an indication of the capability for a layer.

Fig. 7. Generated images of faces after binarizing the CONV4 layer. The layer with increased DOR for each experiment is (a) none, (b) CONV1, (c) CONV2, (d) CONV3, and (e) CONV4, respectively. The DOR is increased by 960 for each experiment except for (a). We can see that increasing the DOR of other layers cannot solve the bottleneck problem introduced by CONV4, but increasing the DOR of CONV4 can.

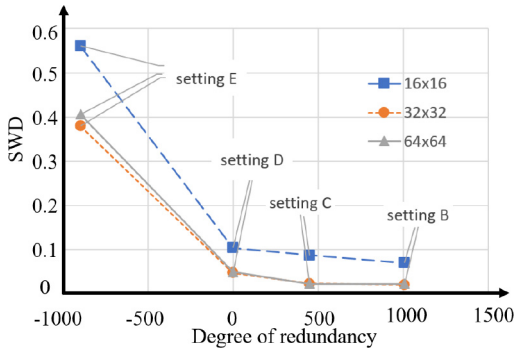

Fig. 8. SWD versus degree of redundancy of the binarized layer in different settings.

In addition, we also conducted the experiments that vary the DOR of the first three layers when binarizing the fourth layer to validate that every layer binarization is relatively independent. In fact, none of these experiments could achieve the same performance improvement as that when increasing the DOR of the fourth layer by a same number. Generated images are shown in Fig. 7.

2) Quantitative Comparison of Single-Layer Binarization: We further quantitatively compute the SWD values with 16×16, 32×32, and 64×64 resolutions for Setting B, Setting C, Setting D, and Setting E. Their relationship with the degree of redundancy of the binarized layer is plotted in Fig. 8. From the figure, two things are clear: first, regardless of resolution, a negative degree of redundancy (Setting E) results in a more than $5\times$ increase in SWD compared with other settings with non-negative degree of redundancy (Setting B, Setting C, and Setting D). Second, for all the three resolutions, SWD decreases almost linearly with the increase of the degree of redundancy when it is non-negative. This confirms that our degree of redundancy can capture the impact of binarization not only on the holistic structure but also on the pixel-level

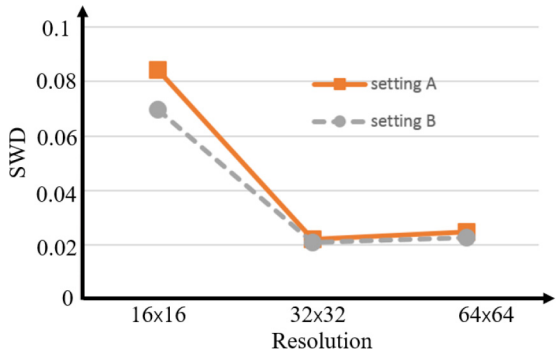

Fig. 9. SWD versus resolution for SWD score calculation under Setting A and Setting B.

TABLE III
AVERAGE SWD UNDER DIFFERENT SETTINGS

Setting	A	B	C	D	E
Average SWD ($\times 10^{-3}$)	44	38	45	67	449

fine details, and as such, is indeed a good indicator to quickly judge whether a layer can be binarized.

We also report the SWD averaged over different resolutions (16×16, 32×32, 64×64) in Table III, where the result for the original GAN (Setting A) is also reported. From the table we can draw similar conclusions, that binarizing second layer (Setting C) increases the average SWD by 2.3% compared with the original GAN (Setting A), while binarizing third and fourth layer (Setting D and Setting E) further increases it by 52.3% and 913.6%, respectively.

It is interesting to note that the average SWD achieved by binarizing the first layer (Setting B) is 13.6% smaller than that from the original DCGAN (Setting A). To further check this, we plot the SWD versus resolution for these two settings in Fig. 9. From the figure we can see that the SWD from Setting B is always smaller than that from Setting A across all three resolutions. This shows that Setting B can achieve better similarity, as well as detailed attributes. Such an improvement is probably due to the regularization effect, and similar effect has been observed in the compression of CNNs [32].

3) Validation of Superposition of Binarizability: We now explore experiments to verify our inference that all layers that can be binarized alone can be binarized together. The images generated by Setting F in Fig. 5(f), where the first three layers in the generator are binarized together, show no significant difference from those in Fig. 5(a)–(d). Binarizing any two layers from the first three layers (not shown here) will lead to the same result. On the other hand, Setting G does not generate any meaningful output [Fig. 5(g)], as the last layer, which cannot be binarized alone, is binarized together with the first three layers. Binarizing any of the first three layers, as well as the last layer (not shown here) will produce meaningless results too. Setting G follows the state-of-the-art binarization for CNNs directly without considering the degree of redundancy. That is, with the assistance of the degree of redundancy, we can figure out that at most the first three deconvolution layers can be binarized with small loss on performance in the generator (Setting F). Nevertheless, directly adopting

Fig. 10. Images generated under different settings using the least-square loss. (a) Setting A. (b) Setting B. (c) Setting C. (d) Setting D. (e) Setting E. (f) Setting F. (g) Setting G. (h) Setting H.

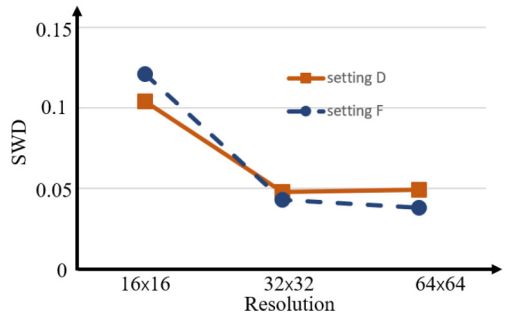

Fig. 11. SWD versus resolutions under Setting D and Setting F.

the existing binarization method will lead to excess degradation in performance and cannot provide any hint to improve (Setting G).

Moreover, the average SWD for Setting F is 0.067, the same as Setting D. Further looking at the SWD values under different resolutions for the two different settings as shown in Fig. 11, it is clear that the two curves are very close. This validates our last inference, that when multiple layers are binarized together, the layer with least degree of redundancy is the bottleneck, which decides the overall performance of the network.

4) Experimental Results Using the Least-Square Loss: The experiments using the least-square loss resulted are in accord with our previous experimental results, as well as conclusions.

For each layer, the performance after binarization decreases along with the layer's redundancy. The images generated by binarizing a single layer in the generator after training using the least-square loss are shown in Fig. 10. Same as in Fig. 5, Fig. 10(a) displays the original results using the least-square loss. Fig. 10(b)–(e) are generated by PBGen's under Setting B—Setting E, respectively, using the least-square loss. As mentioned before, the degree of redundancy of each layer is shown in Fig. 3, which decreases along each layer. As a result, the quality of the generated images also decreases along binarizing each layer under Setting B, Setting C, Setting D, and Setting E. This is the same as that observed in the experiments based on the original loss function in DCGAN.

The superposition of binarizability also holds in the experiments based on the least-square loss. The images generated by Setting F in Fig. 10(f), where the first three layers in the generator are binarized together, show no significant difference from those in Fig. 10(a)–(d). Binarizing any two layers from the first three layers (not shown here) will lead to a similar result. On the other hand, Setting G does not generate any meaningful output [Fig. 10(g)], as the last layer, which cannot be binarized alone, is binarized together with the first three layers. Binarizing any of the first three layers, as well as the last layer (not shown here) will produce meaningless results too. Setting G follows the state-of-the-art binarization for CNNs directly without considering the degree of redundancy based on the least-square loss. That is, with the assistance of the degree of redundancy, we can figure out that at most the first three deconvolution layers can be binarized with small loss on performance in the generator (Setting F) even based on the least-square loss in DCGAN. Nevertheless, directly adopting the existing binarization method will lead to excessive degradation in performance and cannot provide any hint to improve (Setting G), even if a better loss function, the least-square loss, is used.

5) Compression Saving: We also investigate the computation saving during training and inference and memory

TABLE IV
TRAINING AND INFERENCE SPEEDUP, AS WELL AS MEMORY REDUCTION FOR PBGEN

Generator model	Computation Saving		Memory Cost
	Inference	Training	
Original generator from DCGAN (Setting A)	1.0×	1.0×	1.0×
PBGen (Setting F)	∼1.96×	∼1.32×	∼1/25.81×

reduction of partially binarized deconvolution-based generators in hardware designs. Since BWN in [20] is adopted to binarize layers, the same estimation on computation saving and memory cost as BWN is also utilized.

Note that each binarized weight is 32× small over its single precision presentation. Assume that out of a total of N weights, K are binarized. Then the new memory cost can be computed as

$$(K + 32 \times (N - K))/(32 \times N). \tag{3}$$

On the other hand, Rastegari *et al.* [20] mentioned the computation saving is ∼2× after binarization for a standard convolution operation, because multiplication is replaced by only addition and subtraction. This is also the situation when weights are binarized in a deconvolution operation, so the computation saving is adopted for a standard deconvolution operation. That is, the new computation cost can also be calculated using (3) by replacing weights with deconvolution operations, and using 2 instead of 32.

Table IV summarizes the computation saving during training and inference, as well as the memory reduction for PBGen compared with the original generator in DCGAN, which is the baseline model when considering the computation saving and the memory saving. PBGen under Setting F can achieve 25.81× memory saving, as well as 1.96× and 1.32× speedup during inference and training, respectively, with little performance loss. For both the original generator and PBGen, during the training process the floating point representation of all weights need to be used for backward propagation and update [20]. As such, the speedup mainly comes from faster forward propagation with binarized weights.

The relationship between the memory saving and the input channel number of the fourth deconvolution layer (CONV4) on the generator is also investigated. Note that increasing the input channel number of the fourth convolution layer (CONV4) will increase its DOR and at the same time the memory cost. On the other hand, eventually a high enough DOR (above 1024) will enable the layer to be binarized, leading to memory reduction. This can be seen in Fig. 12, where x-axis is the input channel number of CONV4 and the y-axis is the total memory cost of the generator normalized to the original generator without any binarization. Before the input channel number of CONV4 reaches 1024, only the first three deconvolution layers can be binarized, so increasing DOR will result in the quick growth of memory cost. However, when the input channel number of CONV4 is 1024, all the four deconvolution layers can be binarized, which introduces extra memory saving to alleviate the memory cost increment.

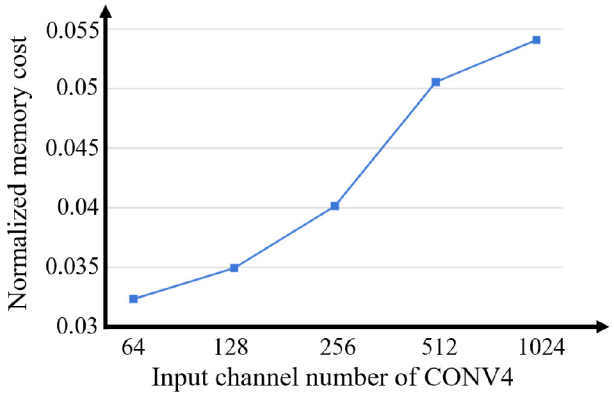

Fig. 12. Memory cost (normalized to the original model without binarization) versus input channel number of CONV4. Before the input channel number of CONV4 reaches 1024, only the first three deconvolution layers can be binarized without significant performance loss, and when the input channel number of CONV4 is 1024, all the four deconvolution layers can be binarized without significant loss.

6) Unbalanced Competition: So far, our discussion has focused on the binarization of the generator in a GAN only, as the discriminator takes the same form as conventional CNNs. However, since competition between generator and discriminator is the key of GANs, would a binarized generator still compete well with a full discriminator?

The loss values for the discriminator network and PBGen under Setting F are depicted in Fig. 13, where x-axis indicates the number of epochs and y-axis is the loss value. The images generated from different number of epochs are also exhibited aside. From the figure we can see that during the initial stage, distorted faces are generated. As the competition is initiated, image quality improves. But very quickly, the competition vanishes, and the generated images stop improving. However, when we binarize the discriminator at the same time (Setting H), the competition continues to improve image quality, as can be seen in Fig. 14.

We further plot the loss values of the discriminator and the generator of the original DCGAN (Setting A), and the results are shown in Fig. 15. It is very similar to Fig. 14, except that the competition is initiated earlier, which is due to the stronger representation power of both the generator and the discriminator before binarization. These figures confirm that the quick disappearance of competition is mainly due to the unbalanced generator and discriminator, which should be avoided.

We now explore the quality of the images generated from balanced competition using Setting H. The images generated are shown in Figs. 5(h) and 10(h), the quality of which is apparently better than the rest in Figs. 5 and 10, respectively. To further confirm this quantitatively, we compute the average SWD values of those images, which is 0.034 in average. This is even smaller than any average SWD values listed in Table III, which shows that the images are of better quality, even compared with the original DCGAN.

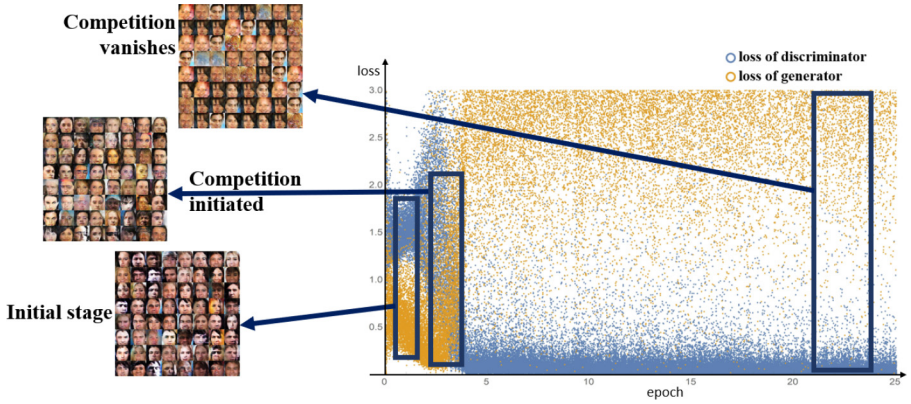

Fig. 13. Loss values of the original discriminator and PBGen under Setting F along epochs.

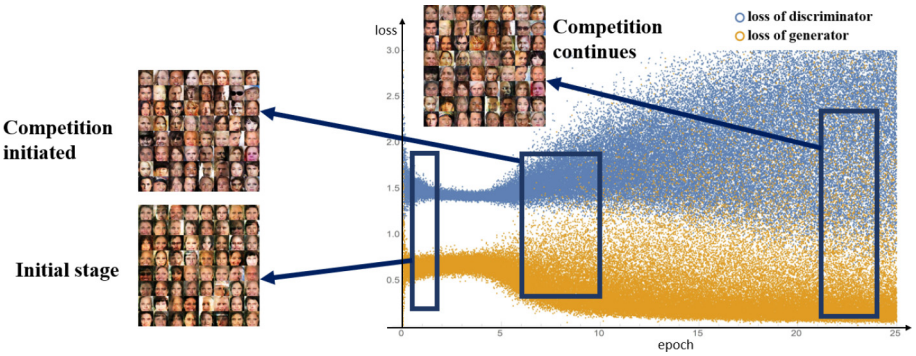

Fig. 14. Loss values of binarized discriminator and PBGen under Setting H along epochs.

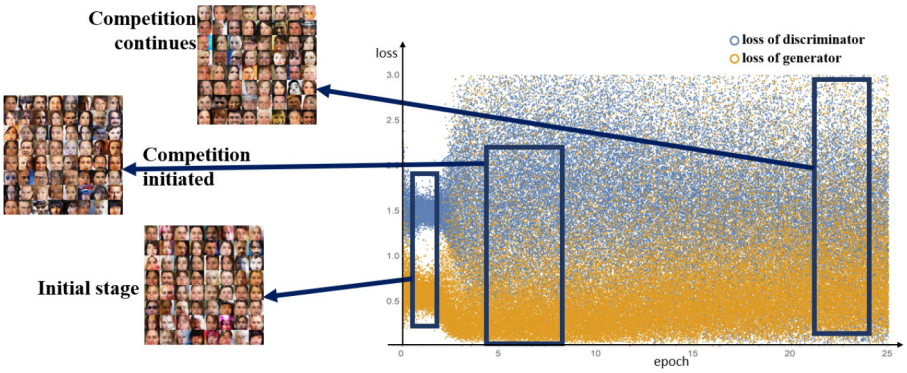

Fig. 15. Loss values of the discriminator and the generator in original DCGAN under Setting A along epochs.

7) Summary: To summarize the discussion and comparisons in this section, we plot the SWD versus resolution curves for all the eight settings in Fig. 16. It allows a complete view of how these different settings compare in terms of similarity as a whole and fine details. From the figure we can see that Setting H gives the best similarity as a whole, while Setting C yields the finest detailed attributes.

Consequently, utilizing the degree of redundancy as a tool, we can efficiently find out eligible layers that can be binarized and based on their superposition, a final binarization strategy can be decided. It cannot guarantee an optimal result but does decrease the search space for the final solution from $O(2^n)$ to $O(n)$ or less, where n is the number of layers, because testing on all combinations of binarization strategy is not necessary and we only need to binarize every single layer with high degree of redundancy to decide the final strategy. Since

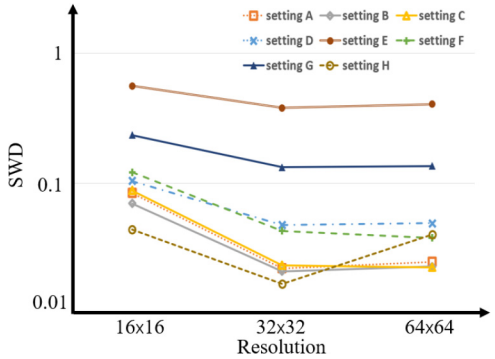

Fig. 16. SWD versus resolutions under all different settings.

our theoretical analysis and experiments are based on deconvolutional layers, we believe this method can work for other deconvolution-based generators beyond DCGAN.

V. Conclusion

Compression techniques have been widely studied for CNNs, but directly adopting them to all layers will fail deconvolution-based generator in generative adversarial networks based on our observation. We propose and validate that the performance of deconvolution-based generator can be preserved when applying binarization to carefully selected layers (PBGen). To accelerate the process deciding whether a layer can be binarized or not, the degree of redundancy is proposed based on theoretical analysis and further verified by experiments. Under the guide of this metric, search space for optimal binarization strategy is decreased from $O(2^n)$ to $O(n)$ where n is the number of layers in the generator. PBGen for DCGAN can yield up to $25.81\times$ saving in memory consumption with $1.96\times$ and $1.32\times$ speedup in inference and training, respectively, with little performance loss measured by SWD score. Besides, we also demonstrate that both generator and discriminator should be binarized at the same time for a balanced competition and better performance.

References

[1] C. Finn, I. Goodfellow, and S. Levine, "Unsupervised learning for physical interaction through video prediction," in *Proc. Int. Conf. Adv. Neural Inf. Process. Syst.*, 2016, pp. 64–72.

[2] D. Pfau and O. Vinyals, "Connecting generative adversarial networks and actor-critic methods," 2016. [Online]. Available: arXiv:1610.01945.

[3] T. Salimans, I. Goodfellow, W. Zaremba, V. Cheung, A. Radford, and X. Chen, "Improved techniques for training GANs," in *Proc. Int. Conf. Adv. Neural Inf. Process. Syst.*, 2016, pp. 2234–2242.

[4] I. Goodfellow, "NIPS 2016 tutorial: Generative adversarial networks," 2016. [Online]. Available: arXiv:1701.00160.

[5] C. Ledig *et al.*, "Photo-realistic single image super-resolution using a generative adversarial network," 2016. [Online]. Available: arXiv:1609.04802.

[6] A. Radford, L. Metz, and S. Chintala, "Unsupervised representation learning with deep convolutional generative adversarial networks," 2015. [Online]. Available: arXiv:1511.06434.

[7] T. Karras, T. Aila, S. Laine, and J. Lehtinen, "Progressive growing of gans for improved quality, stability, and variation," 2017. [Online]. Available: arXiv:1710.10196.

[8] (2017). *Apple Inc*. [Online]. Available: https://www.apple.com

[9] W. Chen, J. Wilson, S. Tyree, K. Weinberger, and Y. Chen, "Compressing neural networks with the hashing trick," in *Proc. Int. Conf. Mach. Learn.*, 2015, pp. 2285–2294.

[10] S. Han, H. Mao, and W. J. Dally, "Deep compression: Compressing deep neural networks with pruning, trained quantization and huffman coding," 2015. [Online]. Available: arXiv:1510.00149.

[11] S. Zhang *et al.*, "Cambricon-X: An accelerator for sparse neural networks," in *Proc. 49th Annu. IEEE/ACM Int. Symp. Microarchitect. (MICRO)*. Taipei, Taiwan, 2016, pp. 1–12.

[12] K. Guo *et al.*, "Angel-Eye: A complete design flow for mapping CNN onto embedded FPGA," *IEEE Trans. Comput.-Aided Design Integr. Circuits Syst.*, vol. 37, no. 1, pp. 35–47, Jan. 2018.

[13] C. Wang, L. Gong, Q. Yu, X. Li, Y. Xie, and X. Zhou, "DLAU: A scalable deep learning accelerator unit on FPGA," *IEEE Trans. Comput.-Aided Design Integr. Circuits Syst.*, vol. 36, no. 3, pp. 513–517, Mar. 2017.

[14] I. Hubara, M. Courbariaux, D. Soudry, R. El-Yaniv, and Y. Bengio, "Quantized neural networks: Training neural networks with low precision weights and activations," 2016. [Online]. Available: arXiv:1609.07061.

[15] A. Al Bahou, G. Karunaratne, R. Andri, L. Cavigelli, and L. Benini, "XNORBIN: A 95 TOp/s/W hardware accelerator for binary convolutional neural networks," in *Proc. IEEE Symp. Low Power High Speed Chips (COOL CHIPS)*, Yokohama, Japan, 2018, pp. 1–3.

[16] F. Li, B. Zhang, and B. Liu, "Ternary weight networks," 2016. [Online]. Available: arXiv:1605.04711.

[17] D. Zhang, J. Yang, D. Ye, and G. Hua, "LQ-Nets: Learned quantization for highly accurate and compact deep neural networks," in *Proc. Eur. Conf. Comput. Vis. (ECCV)*, 2018, pp. 373–390.

[18] F. Conti, P. D. Schiavone, and L. Benini, "XNOR neural engine: A hardware accelerator IP for 21.6-fJ/op binary neural network inference," *IEEE Trans. Comput.-Aided Design Integr. Circuits Syst.*, vol. 37, no. 11, pp. 2940–2951, Nov. 2018.

[19] Y. Ling *et al.*, "TaiJiNet: Towards partial binarized convolutional neural network for embedded systems," in *Proc. IEEE Comput. Soc. Annu. Symp. VLSI (ISVLSI)*, Hong Kong, China, 2018, pp. 136–141.

[20] M. Rastegari, V. Ordonez, J. Redmon, and A. Farhadi, "XNOR-Net: Imagenet classification using binary convolutional neural networks," in *Computer Vision—ECCV*, Cham, Switzerland: Springer, Oct. 2016, pp. 525–542.

[21] S. Han, J. Pool, J. Tran, and W. Dally, "Learning both weights and connections for efficient neural network," in *Proc. Int. Conf. Adv. Neural Inf. Process. Syst.*, 2015, pp. 1135–1143.

[22] N. P. Jouppi *et al.*, "In-datacenter performance analysis of a tensor processing unit," 2017. [Online]. Available: arXiv:1704.04760.

[23] S. Zhou, Y. Wu, Z. Ni, X. Zhou, H. Wen, and Y. Zou, "DoReFa-Net: Training low bitwidth convolutional neural networks with low bitwidth gradients," 2016. [Online]. Available: arXiv:1606.06160.

[24] M. D. Zeiler, D. Krishnan, G. W. Taylor, and R. Fergus, "Deconvolutional networks," in *Proc. IEEE Comput. Soc. Conf. Comput. Vis. Pattern Recognit. (CVPR)*, San Francisco, CA, USA, 2010, pp. 2528–2535.

[25] M. Jaderberg, A. Vedaldi, and A. Zisserman, "Speeding up convolutional neural networks with low rank expansions," 2014. [Online]. Available: arXiv:1405.3866.

[26] M. Lin, Q. Chen, and S. Yan, "Network in network," 2013. [Online]. Available: arXiv:1312.4400.

[27] P. Judd, J. Albericio, T. Hetherington, T. M. Aamodt, and A. Moshovos, "Stripes: Bit-serial deep neural network computing," in *Proc. 49th Annu. IEEE/ACM Int. Symp. Microarchitect. (MICRO)*, Taipei, Taiwan, 2016, pp. 1–12.

[28] D. Miyashita, E. H. Lee, and B. Murmann, "Convolutional neural networks using logarithmic data representation," 2016. [Online]. Available: arXiv:1603.01025.

[29] X. Xu *et al.*, "Quantization of fully convolutional networks for accurate biomedical image segmentation," in *Proc. IEEE Conf. Comput. Vis. Pattern Recognit.*, Salt Lake City, UT, USA, 2018, pp. 8300–8308.

[30] C. Zhu, S. Han, H. Mao, and W. J. Dally, "Trained ternary quantization," 2016. [Online]. Available: arXiv:1612.01064.

[31] A. Zhou, A. Yao, Y. Guo, L. Xu, and Y. Chen, "Incremental network quantization: Towards lossless cnns with low-precision weights," 2017. [Online]. Available: arXiv:1702.03044.

[32] Z. Cai, X. He, J. Sun, and N. Vasconcelos, "Deep learning with low precision by half-wave gaussian quantization," 2017. [Online]. Available: arXiv:1702.00953.

[33] M. Courbariaux, Y. Bengio, and J.-P. David, "BinaryConnect: Training deep neural networks with binary weights during propagations," in *Proc. Int. Conf. Adv. Neural Inf. Process. Syst.*, 2015, pp. 3123–3131.

[34] M. Courbariaux, I. Hubara, D. Soudry, R. El-Yaniv, and Y. Bengio, "Binarized neural networks: Training deep neural networks with weights and activations constrained to $+1$ or -1," 2016. [Online]. Available: arXiv:1602.02830.

[35] Y. Ding, J. Liu, J. Xiong, and Y. Shi, "On the universal approximability and complexity bounds of quantized ReLU neural networks," 2018. [Online]. Available: arXiv:1802.03646.

[36] J. Wang, Q. Lou, X. Zhang, C. Zhu, Y. Lin, and D. Chen, "Design flow of accelerating hybrid extremely low bit-width neural network in embedded FPGA," in *Proc. 28th Int. Conf. Field Program. Logic Appl. (FPL)*, Dublin, Ireland, 2018, pp. 163–1636.

[37] X. Zhu, W. Zhou, and H. Li, "Adaptive layerwise quantization for deep neural network compression," in *Proc. IEEE Int. Conf. Multimedia Expo (ICME)*, San Diego, CA, USA, 2018, pp. 1–6.

[38] S. Yin *et al.*, "A high throughput acceleration for hybrid neural networks with efficient resource management on FPGA," *IEEE Trans. Comput.-Aided Design Integr. Circuits Syst.*, vol. 38, no. 4, pp. 678–691, Apr. 2019.

[39] L. Zhuang, Y. Xu, B. Ni, and H. Xu, "Flexible network binarization with layer-wise priority," 2017. [Online]. Available: arXiv:1709.04344.

[40] X. Xu *et al.*, "Efficient hardware implementation of cellular neural networks with incremental quantization and early exit," *ACM J. Emerg. Technol. Comput. Syst. (JETC)*, vol. 14, no. 4, p. 48, 2018.

[41] I. Chakraborty, D. Roy, A. Ankit, and K. Roy, "Efficient hybrid network architectures for extremely quantized neural networks enabling intelligence at the edge," 2019. [Online]. Available: arXiv:1902.00460.
[42] A. Prabhu, V. Batchu, R. Gajawada, S. A. Munagala, and A. Namboodiri, "Hybrid binary networks: Optimizing for accuracy, efficiency and memory," in *Proc. IEEE Winter Conf. Appl. Comput. Vis. (WACV)*, Lake Tahoe, NV, USA, 2018, pp. 821–829.
[43] I. Chakraborty, D. Roy, I. Garg, A. Ankit, and K. Roy, "PCA-driven hybrid network design for enabling intelligence at the edge," 2019. [Online]. Available: arXiv:1906.01493.
[44] J. Song, "Binary generative adversarial networks for image retrieval," 2017. [Online]. Available: arXiv:1708.04150.
[45] I. Goodfellow *et al.*, "Generative adversarial nets," in *Proc. Int. Conf. Adv. Neural Inf. Process. Syst.*, 2014, pp. 2672–2680.
[46] S. Reed, Z. Akata, X. Yan, L. Logeswaran, B. Schiele, and H. Lee, "Generative adversarial text to image synthesis," 2016. [Online]. Available: arXiv:1605.05396.
[47] X. Chen, Y. Duan, R. Houthooft, J. Schulman, I. Sutskever, and P. Abbeel, "InfoGAN: Interpretable representation learning by information maximizing generative adversarial nets," in *Proc. 30th Int. Conf. Adv. Neural Inf. Process. Syst.*, 2016, pp. 2180–2188.
[48] M. Arjovsky, S. Chintala, and L. Bottou, "Wasserstein generative adversarial networks," in *Proc. Int. Conf. Mach. Learn.*, 2017, pp. 214–223.
[49] X. Mao, Q. Li, H. Xie, R. Y. Lau, Z. Wang, and S. P. Smolley, "Least squares generative adversarial networks," 2016. [Online]. Available: ArXiv:1611.04076.
[50] CS231n Course Materials. (2017). *Implementation as Matrix Multiplication*. [Online]. Available: http://cs231n.github.io/convolutional-networks/#layers
[51] F. N. Iandola, S. Han, M. W. Moskewicz, K. Ashraf, W. J. Dally, and K. Keutzer, "SqueezeNet: Alexnet-level accuracy with 50× fewer parameters and <0.5MB model size," 2016. [Online]. Available: arXiv:1602.07360.
[52] M. Abadi *et al.*, "TensorFlow: Large-scale machine learning on heterogeneous distributed systems," 2016. [Online]. Available: arXiv:1603.04467.
[53] T. Kim. (2017). *DCGAN-Tensorflow*. [Online]. Available: https://github.com/carpedm20/DCGAN-tensorflow
[54] Z. Liu, P. Luo, X. Wang, and X. Tang, "Deep learning face attributes in the wild," in *Proc. Int. Conf. Comput. Vis. (ICCV)*, Santiago, Chile, 2015, pp. 3730–3738.
[55] J. Cha. (2017). *TF.Gans-Comparision*. [Online]. Available: https://github.com/qingshan412/tf.gans-comparison
[56] L. Theis, A. van den Oord, and M. Bethge, "A note on the evaluation of generative models," in *Proc. Int. Conf. Learn. Represent. (ICLR)*, 2016, pp. 1–10.
[57] Y. Wu, Y. Burda, R. Salakhutdinov, and R. Grosse, "On the quantitative analysis of decoder-based generative models," 2016. [Online]. Available: arXiv:1611.04273.
[58] A. Odena, C. Olah, and J. Shlens, "Conditional image synthesis with auxiliary classifier GANs," 2016. [Online]. Available: arXiv:1610.09585.

Jinglan Liu received the B.S. degree in communication engineering from the Beijing University of Posts and Telecommunications, Beijing, China, in 2014. She is currently pursuing the Ph.D. degree with the University of Notre Dame, Notre Dame, IN, USA.

Her current research interests include the applications and acceleration on generative adversarial networks.

Jiaxin Zhang received the B.S. degree in applied physics from the University of Science and Technology of China, Hefei, China, in 2018, and the M.S. degree in electrical and computer engineering from Boston University, Boston, MA, USA, in 2020.

He is currently a Software Engineer with Horizon Robotics, Beijing, China, focusing on computer vision.

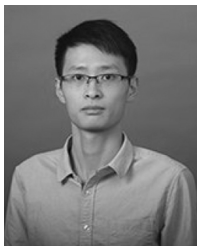

Yukun Ding received the B.S. degree in automation and the M.S. degree in mechanical engineering from the Beijing University of Posts and Telecommunications, Beijing, China, in 2014 and 2017, respectively. He is currently pursuing the Ph.D. degree with the Department of Computer Science and Engineering, University of Notre Dame, Notre Dame, IN, USA.

His current research interests include the application, acceleration, and trustworthiness of deep learning.

Xiaowei Xu (Member, IEEE) received the B.S. and Ph.D. degrees in electronic science and technology from the Huazhong University of Science and Technology, Wuhan, China, in 2011 and 2016, respectively.

He is currently an AI Researcher with Guangdong Provincial People's Hospital, Guangzhou, China. He worked as a Postdoctoral Researcher with the University of Notre Dame, Notre Dame, IN, USA, from 2016 to 2019. His research interests include deep learning, and medical image segmentation.

Dr. Xu was a recipient of the DAC System Design Contest Special Service Recognition Reward in 2018, and the Outstanding Contribution in Reviewing, Integration, the VLSI Journal in 2017. He has served as a TPC members in ICCD, ICCAD, ISVLSI, and ISQED.

Meng Jiang received the B.E. and Ph.D. degrees from the Department of Computer Science and Technology, Tsinghua University, Beijing, China, in 2010 and 2015, respectively.

He is currently an Assistant Professor with the Department of Computer Science and Engineering, University of Notre Dame, Notre Dame, IN, USA. He was a Postdoctoral Research Associate with the University of Illinois at Urbana–Champaign, Urbana, IL, USA, from 2015 to 2017. He has published over 50 papers in top conferences and journals, such as IEEE TRANSACTIONS ON KNOWLEDGE AND DATA ENGINEERING, ACM SIGKDD, AAAI, ACM CIKM, and IEEE ICDM. He has delivered six tutorials in major conferences. His research interests are data mining, knowledge discovery, and machine learning.

Dr. Jiang was a recipient of the Notre Dame Global Gateway Faculty Award. He got the Best Paper Finalist in ACM SIGKDD 2014.

Yiyu Shi (Senior Member, IEEE) received the B.S. degree in electronic engineering from Tsinghua University, Beijing, China, in 2005, and the M.S. and Ph.D. degrees in electrical engineering from the University of California at Los Angeles, Los Angeles, CA, USA, in 2007 and 2009, respectively.

He is currently an Associate Professor with the Department of Computer Science and Engineering, University of Notre Dame, Notre Dame, IN, USA, where he is the Site Director of the NSF I/UCRC Alternative and Sustainable Intelligent Computing and the Director of the Sustainable Computing Laboratory. His current research interests focus on hardware intelligence and biomedical applications. In recognition of his research, many of his papers have been nominated for the Best Paper Awards in top conferences.

Dr. Shi was also a recipient of NSF CAREER Award, IEEE Region Five Outstanding Individual Achievement Award, and the IEEE TCVLSI Mid-Career Research Award. He is an associate editor of various IEEE/ACM journals. He is the Education Chair of ACM SIGDA and the Deputy Editor-in-Chief of IEEE VLSI CAS Newsletter.